Copy 5
RM E52G29

NACA RM E52G29

RESEARCH MEMORANDUM

ALTITUDE INVESTIGATION OF THREE FLAME-HOLDER AND FUEL-SYSTEMS CONFIGURATIONS IN A SHORT CONVERGING AFTERBURNER ON A TURBOJET ENGINE

By Willis M. Braithwaite, Paul E. Renas, and Emmert T. Jansen

Lewis Flight Propulsion Laboratory
Cleveland, Ohio

NATIONAL ADVISORY COMMITTEE
FOR AERONAUTICS

WASHINGTON

September 10, 1952

NACA RM E52G29

NATIONAL ADVISORY COMMITTEE FOR AERONAUTICS

RESEARCH MEMORANDUM

ALTITUDE INVESTIGATION OF THREE FLAME-HOLDER AND FUEL-SYSTEMS CONFIGURATIONS IN A SHORT CONVERGING AFTERBURNER ON A TURBOJET ENGINE

By Willis M. Braithwaite, Paul E. Renas, and Emmert T. Jansen

SUMMARY

An investigation was conducted in an altitude chamber at the NACA Lewis laboratory to evaluate an internal afterburner configuration for a turbojet engine having a short converging conical afterburner shell with a two-position exhaust nozzle. Three configurations, which were designed on the basis of previous experiments with this burner, were installed. Performance characteristics and operational limits of each were obtained over a range of altitudes to determine which configuration best satisfied the design requirement that the burner operate satisfactorily up to an altitude of 50,000 feet.

An afterburner configuration was designed that had an altitude operational limit of 51,000 feet with essentially no effect of altitude on performance up to an altitude of 45,000 feet. In order to obtain this performance, the afterburner internal configuration which included a two-ring V-gutter flame holder, a streamlined diffuser inner body, and 16 fuel bars had to be further modified to include 37 turbine-outlet gas-flow straightening vanes.

INTRODUCTION

Operational requirements of recent interceptors or other high-performance aircraft demand satisfactory turbojet-engine operation at increasingly higher flight speeds and altitudes. In accordance with these requirements, the present investigation, which was conducted in an altitude chamber at the NACA Lewis laboratory, was directed toward obtaining satisfactory afterburner performance and operational characteristics for a particular engine-afterburner combination up to an altitude of 50,000 feet. The engine-afterburner combination used for this investigation consisted of a preproduction power section, a short

afterburner, and a two-position clamshell nozzle as supplied by the engine manufacturer. The outer shell of the afterburner remained unaltered throughout the investigation.

Previous investigations of a number of internal configurations in the same afterburner shell are reported in references 1 and 2. From this information, a two-ring V-gutter flame holder had been incorporated in the design of the afterburner used in this investigation. The diffuser inner body had also been modified in order to provide an improved velocity profile at the burner inlet. In the investigation reported herein, the performance and operational characteristics of three afterburner internal configurations were evaluated. Turbine-outlet guide vanes were installed for one of the three configurations to reduce the amount of swirl in the gas flow entering the burner from the turbine.

Operational characteristics of the three afterburner configurations and altitude performance of two of the three configurations are presented in both tabular and graphical form. Performance data were obtained over a range of altitudes from 10,000 to 45,000 feet for the initial and final configurations, and performance data were obtained over a range of flight Mach numbers at an altitude of 30,000 feet for the final configuration.

APPARATUS

Installation

The engine was installed in an altitude chamber which is 10 feet in diameter and 60 feet long (fig. 1). A honeycomb is installed in the chamber upstream of the test section to straighten and to smooth the flow of inlet air. The forward bulkhead, which incorporates a labyrinth seal around the forward end of the engine, was used to separate the engine-inlet air from the exhaust and to provide a means of maintaining a pressure difference across the engine. A 14-inch butterfly valve was installed in the forward bulkhead to provide cooling air for the engine compartment. The rear bulkhead was installed to prevent recirculation of exhaust gases about the engine. The exhaust gas from the jet nozzle was discharged into an exhaust diffuser to recover some of the kinetic energy of the jet. Combustion in the afterburner was observed through a periscope located directly behind the engine.

Engine

A J35-A-35 engine, which includes the afterburner, was used in this investigation. The engine has a static sea-level thrust rating of 5400 pounds without afterburning (5600 lb without compressor-inlet

screens) at rated engine speed of 8000 rpm and a turbine-outlet temperature of 1300° F, for an inlet-air temperature of 60° F (reference 3). At this operating condition, the air flow is 91 pounds per second and the specific fuel consumption is 1.09 pounds per hour per pound of thrust. The principal components of the engine are an 11-stage axial-flow compressor, eight cylindrical through-flow combustion chambers, a single-stage turbine, and an afterburner. The over-all length of the engine and afterburner is approximately 196 inches and the maximum diameter is 43 inches. Throughout the investigation MIL-F-5624A, grade JP-3, fuel with a low heating value of 18,750 Btu per pound and a hydrogen-carbon ratio of 0.171 was used in both the engine and the afterburner.

Afterburner Assembly

Cross sections of the afterburner assemblies used are shown in figure 2. The afterburner shell, common to all configurations investigated, was $76\frac{3}{16}$ inches long and was composed of three sections: (1) a conical diffuser followed by a short cylindrical section, (2) a converging conical burning section, and (3) a two-position clamshell-type nozzle. The two-position nozzle was maintained in the open position (area, 389 sq in.) throughout the investigation. Fuel was supplied to the afterburner by an air-turbine fuel pump which was driven by air from an independent source.

The three configurations reported herein included the variations listed in the following table:

Configuration	Fuel System			Flame holder			
	Number of fuel-spray bars	Orifices per spray bar	Mixing length (in.)	Type	Distance from nozzle outlet (in.)	Blocked area (percent of flow area)	Blocked area (percent of afterburner cross-sectional area)
A	16	[a]9	$6\frac{1}{4}$	2-V ring; pilot on inner body	$44\frac{9}{16}$	37.5	37.5
B	16	10	$9\frac{1}{4}$	2-V ring; dome on inner body	$49\frac{11}{16}$	42.2	35.9
C	16	10	$9\frac{1}{4}$	2-V ring; dome on inner body	$49\frac{11}{16}$	42.2	35.9

[a]One orifice was drilled in the end of each fuel bar to supply fuel for the diffuser-inner-body flame seat (fig. 3).

[redacted]

The diffuser inner body for configuration A was supported from the outer wall by four rods which were covered by faired struts having a chord length of $7\frac{1}{2}$ inches (fig. 2(a)). The downstream end of this diffuser contained a depressed flame seat $11\frac{7}{8}$ inches in diameter. The flame holder was mounted from the outer shell and located $3\frac{1}{2}$ inches downstream of the inner body. From the inner ring of this flame holder, six stubs $1\frac{1}{2}$ inches long protruded inward (fig. 2(a)). The fuel systems for all configurations are shown in figure 3.

For configuration B, the faired struts were removed leaving the bare support rods, and the flame seat was replaced by a dome (figs. 2(a) and 4). The flame holder was the same as for configuration A except that the six stubs were replaced by four supporting struts attached to the dome of the diffuser inner body (fig. 4). The flame holder was also moved forward $3\frac{1}{2}$ inches (fig. 2(b)). The fuel system for this configuration is shown in figure 3(b).

Configuration C had the same inner body with rod supports, flameholder mounting and location, and fuel system as configuration B. In addition, 37 evenly spaced flow-straightening vanes (fig. 5) were installed at the turbine outlet on the diffuser body. These vanes were designed to turn the flow leaving the turbine approximately 40° at the turbine blade root to 0° at the blade tip (fig. 5(b)).

The afterburner hot-streak ignition system consisted of two fuel nozzles approximately 180° apart located just aft of the downstream side of the turbine. These nozzles injected fuel into the turbine-outlet gas stream about two inches from the outer shell only during the ignition cycle.

Instrumentation

Engine-inlet air flow was determined by temperature, total-pressure survey rakes, and wall static-pressure orifices located at the compressor inlet (station 1, fig. 6(a)). Instrumentation was installed for measuring the engine midframe air bleed. This air flow was subtracted from the engine-inlet air flow in order to obtain the afterburner air flow. Afterburner-inlet total pressure and temperature were determined from a survey at the turbine outlet (station 5, fig. 6(b)). Turbine-outlet temperature was also measured by the engine manufacturer's instrumentation, which consisted of a thermocouple harness comprised of 10 thermocouples. Static pressures were measured at the diffuser outlet by wall orifices. Total pressures were measured at the

exhaust-nozzle inlet with a water-cooled survey rake (fig. 6(c)). The angle of swirl of the gas flow was measured at the exhaust-nozzle inlet by means of a water-cooled rotatable rake (fig. 6(d)). The rake was equipped with an actuator that positioned the probes at an angle to the plane of the axis of the engine. Ambient pressure in the region of the exhaust-nozzle outlet was determined by static probes in the plane of the nozzle outlet. Engine and afterburner fuel flows were measured by calibrated rotameters.

PROCEDURE

Afterburner operational and performance data were obtained over a range of altitudes from 10,000 feet to the maximum operable altitude at a flight Mach number of 0.6 and over a range of flight Mach numbers from 0.4 to 0.8 at an altitude of 30,000 feet. For each flight condition, data were obtained at several afterburner fuel flows between the lean blow-out limit and the fuel flow required for limiting turbine-outlet temperature (1760° R). The lean operating limit was determined by: (1) complete blow-out of the burner, (2) rough burning, or (3) flame seating only in the pilot burner (configuration A). Limiting turbine-outlet temperature was defined as operation at 1300° F (1760° R) as indicated by the manufacturer's instrumentation. All afterburning data were obtained with the engine operating at rated speed (8000 rpm) and with the two-position nozzle in the open position. Engine-inlet-air total temperature and total pressure were regulated to correspond to NACA standard altitude conditions.

The procedure followed in the ignition investigation was to close the eyelids of the exhaust nozzle and to inject fuel into the afterburner and through the hot-streak fuel nozzle. As soon as the turbine-outlet temperature started to increase, the eyelids of the nozzle were opened and the hot-streak ignition fuel was shut off.

The methods and symbols used in the calculations are given in the appendix.

RESULTS AND DISCUSSION

Operational Characteristics

The operational limits of the three configurations are presented in figure 7 for varying altitude and flight Mach number. The two basic operational limits which are presented are: (1) afterburner lean operating limit, and (2) limiting turbine-outlet temperature operation. The maximum altitude limit, which is defined as lean combustion blow-out at limiting turbine-outlet temperature, is also presented.

The first of the three configurations investigated (configuration A) had an altitude limit of approximately 47,000 feet at an afterburner fuel-air ratio of 0.049. Because the primary objective of this investigation was the development of an afterburner that would operate at an altitude of 50,000 feet, this configuration was considered unsatisfactory. Along with failure to reach the desired altitude, another disadvantage of this configuration was burning in the wake of the diffuser struts with a resultant short service life of the downstream end of the inner body, which was caused by the high degree of swirl of the gases leaving the turbine. Consequently, the faired struts were removed and the flame holder moved to the end of the diffuser with a dome replacing the flame seat (configuration B). The maximum altitude obtained with this configuration was approximately 41,500 feet at a fuel-air ratio of 0.0315. At this condition, visual observation indicated a very unstable and swirling flame.

Measurements by the engine manufacturer at sea-level static conditions (fig. 8(a)) and flame patterns on the inner body indicated that the swirl angle leaving the turbine varied linearly from approximately 40° at the blade root to approximately 0° at the tip in a direction opposite to the rotation of the turbine rotor. Because the gases are entering a diffusing section, the angle of swirl of the gases downstream from this station can be expected to be as great if not greater than those indicated previously.

In order to reduce the swirl angle of the gases leaving the turbine, straightening vanes were installed at the turbine outlet (configuration C). With this configuration change, the swirl angle was reduced to less than 10° at the center of the exhaust-nozzle inlet as was indicated by a survey at this station (fig. 8(a)). These data were obtained by rotating the rake in such a manner that the probes were at the various angles to the plane of the engine axis and were evaluated as shown in figures 8(a) and 8(b).

This configuration (configuration C) had an altitude limit of approximately 51,000 feet (fig. 7), improved afterburner performance, increased service life, and improved stability of combustion (less flickering of the visible flame). Ignition of the afterburner was possible with the torch igniter provided by the engine manufacturer for the range of altitudes covered in this investigation.

Performance Characteristics

Altitude performance data are presented in tabular form in table I and in graphical form in figures 9 to 13. Figure 9 presents a comparison of the performance of configurations A and C at altitudes of 30,000 and 40,000 feet for a flight Mach number of 0.6. Figures 10

and 11 present data for configuration C for a range of altitudes at a flight Mach number of 0.6 and a range of flight Mach numbers at an altitude of 30,000 feet. Figures 12 and 13 present the over-all engine performance for configuration C.

Comparison of configurations. - The afterburner-inlet conditions for configurations A and C are presented in figures 9(a) and 9(b) and the afterburner performance is shown in figures 9(c) to 9(f). Performance data could not be obtained for configuration B because of the high degree of swirl which prevented an accurate measurement of pressures; however, the performance of this configuration is not considered of importance because of the poor altitude operational characteristics.

For a given afterburner fuel-air ratio, configuration A had a lower turbine-outlet temperature but a higher total pressure than configuration C. The turbine-outlet total pressure is lower for configuration C because of the pressure drop across the straightening vanes. A comparison of the performance for these two configurations shows that for configuration C the afterburner combustion efficiency, exhaust-gas total temperature, and augmented net thrust is higher and specific fuel consumption is lower than the corresponding values for configuration A. The magnitude of the difference is indicated by the combustion efficiency which increased from 0.86 for configuration A to 0.91 for configuration C.

Altitude and flight Mach number effects. - The performance obtained for configuration C over a range of altitudes from 10,000 to 45,000 feet at a flight Mach number of 0.6 is shown in figure 10 and the effect of varying flight Mach number from 0.4 to 0.8 at an altitude of 30,000 feet is shown in figure 11. For a given afterburner fuel-air ratio, increasing the altitude at a constant flight, or decreasing the flight Mach number at a constant altitude, tended to lower the turbine-outlet total temperature and to reduce the turbine-outlet total pressure in proportion to the compressor-inlet total pressure. In addition, increasing altitude had no appreciable effect on afterburner combustion efficiency, exhaust-gas total temperature, or specific fuel consumption, but reduced the augmented net thrust. A peak afterburner combustion efficiency of approximately 91 percent was obtained with this burner up to an altitude of 45,000 feet.

Because the turbine-outlet total temperature decreased as the altitude increased, or flight Mach number increased, it would be expected that the exhaust-gas total temperature would decrease if the afterburner combustion efficiency were constant. However, the afterburner fuel-air ratio is defined (see appendix) as the ratio of the afterburner fuel to the total air less the air used for complete combustion of the primary engine fuel. Because the engine combustion is not 100 percent efficient, some unburned fuel from the engine enters

the afterburner along with the unburned air and products of combustion. This quantity of unburned fuel is not accounted for in the afterburner fuel-air ratio. Therefore, for the same afterburner combustion efficiency, the temperature rise between the turbine outlet and the nozzle inlet is greater than it would be for the afterburner fuel flow alone. That part of the temperature rise attributed to the unburned engine fuel must be of the same magnitude as the decrease in temperature at the turbine outlet to yield the nozzle-inlet total temperature observed. Examination of the data shows that the temperature rise in the afterburner due to unburned engine fuel for varying flight conditions is of the proper magnitude to give an approximately constant exhaust-gas temperature for any given afterburner fuel-air ratio. The spread in the curves of exhaust-gas temperature and afterburner combustion efficiency is within the normal accuracy of this type of data.

For the range of conditions investigated, the afterburner-combustion-chamber inlet (diffuser outlet) velocity varied from 507 to 463 feet per second as the altitude was increased from 10,000 to 45,000 feet at a flight Mach number of 0.6 and from 485 to 495 feet per second as the flight Mach number was increased from 0.4 to 0.8 at an altitude of 30,000 feet.

Over-All Performance

The over-all performance obtained with configuration C is presented in figures 12 and 13 for a turbine-outlet gas temperature of 1710° R, based on NACA thermocouple instrumentation, which is the highest temperature at which data were available at all conditions for cross plotting. It must be emphasized that the performance data presented are significant only for an exhaust-nozzle area of 389 square inches as used in this investigation. The relation of the manufacturer's indicated turbine-outlet temperature to a NACA turbine-outlet total temperature of 1710° R is presented in figures 12(d) and 13(d) for varying altitude and flight Mach number, respectively. Exhaust-gas total temperature, augmented thrust ratio, and specific fuel consumption are shown in figure 12 for a range of altitudes at a flight Mach number of 0.6. The augmented thrust ratio is defined as the net thrust obtained with afterburning to the net thrust obtained with the engine and standard tail pipe at a turbine-outlet gas temperature of 1710° R. For a change in altitude from 10,000 to 45,000 feet at a flight Mach number of 0.6, constant exhaust-nozzle-area afterburner operation at a turbine-outlet total temperature of 1710° R resulted in an increase in exhaust-gas temperature from 2810° to 3300° R, an increase in augmented thrust ratio from 1.42 to 1.56, and essentially no change in specific fuel consumption. If the afterburner were operated at constant fuel-air ratio as the altitude was increased, the turbine-outlet gas temperature would decrease. Therefore, in order to maintain constant turbine-outlet

temperature, additional fuel must be burned in the afterburner which increased the exhaust-gas temperature. For the range of altitude operation from 10,000 to 45,000 feet, the afterburner inoperative thrust loss varies from 1 to $1\frac{1}{2}$ percent of the normal standard engine thrust.

Afterburner performance is shown in figure 13 for a range of flight Mach numbers at an altitude of 30,000 feet with the engine afterburner operating at a fixed exhaust-nozzle area and a turbine-outlet total temperature of 1710° R. An increase in flight Mach number from 0.4 to 0.8 caused a decrease in the exhaust-gas temperature from 3050° to 2970° R and an increase in the augmented thrust ratio from 1.42 to 1.51 while the specific fuel consumption remained approximately constant. The thrust loss with the afterburner inoperative was 1 percent of the standard engine thrust.

CONCLUDING REMARKS

An investigation of a J35-A-35 turbojet engine with a short converging conical afterburner having a two-position exhaust nozzle showed that a severe swirl in the turbine-outlet gases of approximately 40° at the turbine blade root to 0° at the tip can have a detrimental effect upon afterburner performance and operating limits. Modification of the afterburner by the addition of simple straightening vanes immediately downstream of the turbine outlet reduced the swirl angle of the gases entering the burner to less than 10°. This reduction in swirl resulted in improved afterburner performance, altitude limits, flame stability, and service life.

An afterburner combustion efficiency of approximately 90 percent was obtained with the best configuration while no significant altitude effects were observed on afterburner combustion efficiency, exhaust-gas temperature, and net-thrust specific fuel consumption for a change in altitude up to 45,000 feet nor for a change in flight Mach number from 0.4 to 0.8 at 30,000 feet. An altitude limit of 51,000 feet at a flight Mach number of 0.6 was obtained for the final afterburner configuration and combustion was stable up to the point of blow-out.

The rich limit for afterburner operation was limited by maximum allowable turbine-outlet temperature for all the conditions investigated and no rich blow-out was encountered. A larger exhaust nozzle could therefore be used with resulting wider operating range, higher augmented thrust, and possible higher altitude limit.

Lewis Flight Propulsion Laboratory
National Advisory Committee for Aeronautics
Cleveland, Ohio

APPENDIX - CALCULATIONS

Symbols

The following symbols are used in the calculations and on the figures.

A	cross-sectional area, sq ft
C_d	flow coefficient at vena contracta
C_V	velocity coefficient, ratio of actual jet velocity to effective jet velocity
C_T	thermoexpansion ratio, ratio of hot exhaust-nozzle area to cold exhaust-nozzle area
F_j	jet thrust, lb
F_n	net thrust, lb
f/a	fuel-air ratio
g	acceleration due to gravity, 32.2 ft/sec^2
H	total enthalpy, Btu/lb
h_c	lower heating value of fuel, Btu/lb
M	Mach number
N	engine speed, rpm
P	total pressure, lb/sq ft absolute
P_9'	total pressure at exhaust-nozzle survey station in standard engine tail pipe, lb/sq ft absolute
p	static pressure, lb/sq ft absolute
R	gas constant, 53.4 (ft)(lb)/(lb)($^\circ$R)
T	total temperature, $^\circ$R
T_i	indicated temperature, $^\circ$R
t	static temperature, $^\circ$R

[redacted]

V	velocity, ft/sec
W_a	air flow, lb/sec
W_c	compressor leakage air flow, lb/sec
W_f	fuel flow, lb/hr
W_f/F_n	specific fuel consumption based on total fuel flow and net thrust, lb/(hr)(lb thrust)
W_g	gas flow, lb/sec
γ	ratio of specific heats for gases
η_b	afterburner combustion efficiency
η_e	engine combustor efficiency

Subscripts:

a	air
e	engine
f	fuel
g	gas
i	indicated by instrumentation
j	station at which static pressure of jet equals free-stream static pressure
m	fuel manifold
n	exhaust-nozzle outlet, vena contracta
t	tail-pipe afterburner
0	free-stream conditions
1	engine inlet
3	compressor outlet at engine-combustor inlet
5	turbine outlet or tail-pipe diffuser inlet

[redacted]

6 diffuser outlet at tail-pipe combustion-chamber inlet, leading edge of flame holder

9 exhaust-nozzle inlet, $3\frac{1}{5}$ inches upstream of nozzle outlet

10 exhaust-nozzle outlet

Methods of Calculation

Temperatures. - Static temperatures were determined from indicated temperatures using the relation

$$t = \frac{T_1}{1 + 0.95\left[\left(\frac{P}{p}\right)^{\frac{\gamma-1}{\gamma}} - 1\right]}$$

where 0.95 is the impact recovery factor for the type of thermocouple used.

Flight Mach number and airspeed. - Flight Mach number and equivalent airspeed were calculated from engine-inlet total pressure and total temperature and free-stream static pressure assuming complete total-pressure ram recovery:

$$M_0 = \sqrt{\frac{2}{\gamma_1-1}\left[\left(\frac{P_1}{p_0}\right)^{\frac{\gamma_1-1}{\gamma_1}} - 1\right]}$$

and

$$V_0 = M_0\sqrt{\gamma_1 g\, RT_1\left(\frac{p_0}{P_1}\right)^{\frac{\gamma_1-1}{\gamma_1}}}$$

Air flow. - Air flow was determined from pressure and temperature measurements obtained in the engine-inlet annulus. These measurements were used in the following equation

$$W_{a,1} = p_1 A_1\sqrt{\frac{2\gamma_1 g}{(\gamma_1-1)Rt_1}\left[\left(\frac{P_1}{p_1}\right)^{\frac{\gamma_1-1}{\gamma_1}} - 1\right]}$$

[redacted]

Air flow at the compressor outlet (station 3) was obtained by subtracting the compressor leakage air flow:

$$W_{a,3} = W_{a,1} - W_c$$

Gas flow. - Engine gas flow at the turbine outlet is

$$W_{g,5} = W_{a,3} + \frac{W_{f,e}}{3600}$$

and afterburner gas flow is

$$W_{g,9} = W_{a,3} + \frac{W_{f,e} + W_{f,t}}{3600}$$

Fuel-air ratio. - The engine fuel-air ratio is given by the equation

$$(f/a)_e = \frac{W_{f,e}}{3600\ W_{a,3}}$$

The tail-pipe afterburner fuel-air ratio used herein is defined as the weight flow of fuel injected into the afterburner divided by the weight flow of unburned air entering the tail-pipe afterburner. Weight flow of unburned air was determined with the use of the assumption that the fuel injected in the engine combustor was completely burned. When air flow, engine fuel flow, and afterburner fuel flow are combined, the following equation for tail-pipe fuel-air ratio is obtained:

$$(f/a)_t = \frac{W_{f,t}}{3600\ W_{a,3} - \frac{W_{f,e}}{0.068}}$$

where 0.068 is the stoichiometric fuel-air ratio for the engine fuel. The total fuel-air ratio for the engine and afterburner is

$$(f/a) = \frac{W_{f,e} + W_{f,t}}{3600\ W_{a,3}}$$

Combustion-chamber inlet velocity. - Velocity at the combustion-chamber inlet was calculated from the continuity equation with the use of the static pressure measured at station 6 and with the assumption of isentropic expansion between stations 5 and 6.

[redacted]

$$V_6 = \frac{W_{g,5}\, RT_5}{p_6\, A_6}\left(\frac{p_6}{P_5}\right)^{\frac{\gamma_5-1}{\gamma_5}}$$

Engine combustor efficiency. - Engine combustor efficiency is the ratio of enthalpy rise through the engine divided by the product of engine fuel flow and the lower heating value of the fuel:

$$\eta_e = \frac{\left[3600\, W_{a,3} H_a\right]_{T_1}^{T_5} + \left[W_{f,e} H_{f,e}\right]_{T_m}^{T_5}}{W_{f,e} h_{c,e}}$$

Afterburner combustion efficiency. - Afterburner combustion efficiency was obtained by dividing the enthalpy rise through the afterburner by the product of afterburner fuel flow and lower heating value of the fuel:

$$\eta_b = \frac{\left[3600\, W_{a,3} H_a\right]_{T_1}^{T_n} + \left[W_{f,e} H_{f,e}\right]_{T_m}^{T_n} + \left[W_{f,t} H_{f,t}\right]_{T_m}^{T_n} - \eta_e W_{f,e} h_{c,e}}{W_{f,t} h_{c,t} + (1 - \eta_e)\, W_{f,e} h_{c,e}}$$

The enthalpy of the combustion products was determined from the hydrogen-carbon ratio of the fuels by the method explained in reference 4, in which dissociation is disregarded.

Exhaust-gas total temperature. - The total temperature of the exhaust gas was calculated from conditions existing at the exhaust-nozzle vena contracta by the air-flow equation:

$$T_n = \left(\frac{p_n C_d C_T A_{10}}{W_{g,9}}\right)^2 \frac{2\gamma_n}{\gamma_n - 1}\frac{g}{R}\left[1 - \left(\frac{p_n}{P_9}\right)^{\frac{\gamma_n-1}{\gamma_n}}\right]$$

The thermal-expansion ratio C_T was based on exhaust-nozzle skin temperature and properties of the metal. The flow coefficient C_d was determined from nonafterburning engine data obtained with the engine-afterburner configuration and is presented in the following figure.

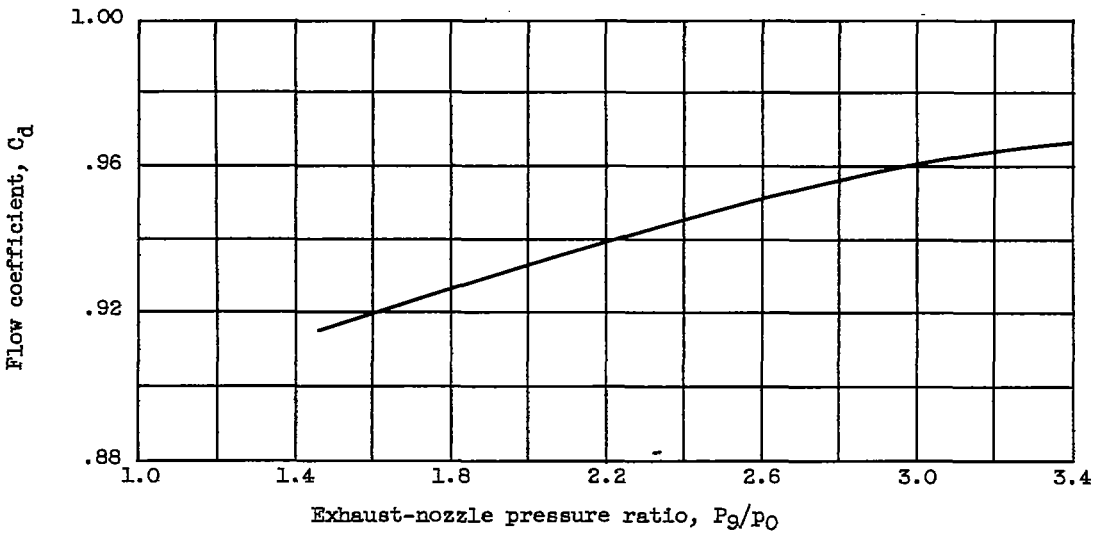

Augmented thrust. - The jet thrust of the combined engine-afterburner configuration was calculated from exhaust-nozzle pressure ratio, exhaust-nozzle gas temperature, and afterburner gas flow.

$$F_j = C_V \left[\frac{W_{g,9}}{g} V_n + A_n (p_n - p_0) \right]$$

where

$$V_n = \sqrt{\frac{2\gamma_n}{\gamma_n - 1} gRT_n \left[1 - \left(\frac{p_n}{P_9} \right)^{\frac{\gamma_n - 1}{\gamma_n}} \right]}$$

The velocity coefficient C_V as determined from previous engine operation was 0.97. The charts in reference 5 were used in the solution of the preceding equation.

The augmented net thrust was obtained by subtracting the free-stream momentum of the inlet air from the jet thrust of the installation.

$$F_n = F_j - \frac{W_{a,1}}{g} V_0$$

[redacted]

Standard engine thrust. - The jet thrust obtainable with the standard engine at rated engine speed was calculated from measurements of turbine-outlet total pressure and total temperature and engine gas flow obtained during the afterburning program:

$$F_{j,e} = C_V \left[\frac{W_{g,5}}{g} V_n + A_n (p_n - p_0) \right]$$

where

$$V_n = \sqrt{\frac{2\gamma_6}{\gamma_6 - 1} gRT_5 \left[1 - \left(\frac{p_n}{P_9'} \right)^{\frac{\gamma_5 - 1}{\gamma_5}} \right]}$$

Experimental data from previous operation of the engine (reference 3) indicated that the total-pressure loss across the standard-engine tail pipe between stations 5 and 9 was approximately 0.025 P_5 at rated engine speed; therefore, $P_9' = 0.0975\ P_5$. The nozzle velocity coefficient was assumed to be 0.97, the same as for the augmented jet thrust.

2607

REFERENCES

1. Grey, Ralph E., Krull, H. G., and Sargent, A. F.: Altitude Investigation of 16 Flame-Holder and Fuel-System Configurations in Tail-Pipe Burner. NACA RM E51E03, 1951.

2. Huntley, S. C., and Wilsted, H. D.: Altitude Performance Investigation of Two Flame-Holder and Fuel-System Configurations in Short Afterburner. NACA RM E52B25, 1952.

3. Walker, Curtis L., Huntley, S. C., and Braithwaite, W. M.: Component and Over-All Performance Evaluation of an Axial-Flow Turbojet Engine over a Range of Engine-Inlet Reynolds Numbers. NACA RM E52B08, 1952.

4. Turner, L. Richard, and Bogart, Donald: Constant-Pressure Combustion Charts Including Effects of Diluent Addition. NACA Rep. 937, 1949. (Supersedes NACA TN's 1086 and 1655.)

5. Turner, L. Richard, Addie, Albert N., and Zimmerman, Richard H.: Charts for the Analysis of One-Dimensional Steady Compressible Flow. NACA TN 1419, 1948.

[redacted]

TABLE I - AFTERBURNER PERFORMANCE DATA

Run	Altitude (ft)	Flight Mach number M_0	Free-stream static pressure p_0 (lb/sq ft abs)	Engine-inlet total pressure P_1 (lb/sq ft abs)	Engine-inlet total temperature T_1 ($^{\circ}R$)	Engine-inlet air flow $W_{a,1}$ (lb/sec)	Engine fuel flow $W_{f,e}$ (lb/hr)	Afterburner fuel flow $W_{f,t}$ (lb/hr)	Total fuel-air ratio f/a	Afterburner fuel-air ratio $(f/a)_t$	Augmented jet thrust F_j (lb)	Net thrust F_n (lb)
Configuration A												
1	30,000	0.606	622	799	448	37.22	2527	4870	0.0561	0.0516	3690	2986
2		.602	624	797	428	38.22	2429	3910	.0467	.0392	3527	2829
3		.595	628	798	437	37.68	2413	3820	.0467	.0391	3505	2815
4		.602	623	796	437	37.61	2283	3350	.0422	.0356	3318	2822
5	40,000	0.595	389	494	421	23.69	1708	2905	0.0550	0.0496	2544	1918
6		.597	391	498	413	23.95	1662	2660	.0509	.0441	2542	1915
7		.613	388	500	417	24.15	1617	2525	.0484	.0410	2288	1844
8		.608	388	488	418	23.98	1585	2405	.0470	.0391	2253	1815
9		.618	386	500	418	23.80	1556	2220	.0447	.0382	2187	1745
Configuration C												
10	10,000	0.618	1434	1852	538	76.19	4355	5910	0.0380	0.0288	6065	4465
11		.634	1419	1859	536	77.03	4249	5455	.0358	.0280	5961	4306
12		.611	1450	1866	541	76.88	3755	4785	.0313	.0220	5068	3482
13		.615	1438	1855	538	77.09	3444	4380	.0286	.0187	4720	3107
14	30,000	0.418	628	705	428	33.25	2268	3450	0.0486	0.0410	3025	2595
15		.401	633	707	425	33.45	2155	2975	.0433	.0344	2856	2441
16		.407	627	703	425	33.53	2076	2710	.0405	.0310	2748	2328
17		.411	627	705	426	33.58	1974	2480	.0377	.0278	2597	2171
18	30,000	0.611	629	810	437	37.94	2514	3890	0.0477	0.0401	3617	2803
19		.610	627	806	450	37.15	2368	3360	.0435	.0348	3359	2653
20		.618	627	811	446	37.48	2268	3010	.0398	.0304	3222	2504
21		.615	626	809	450	37.23	1974	2570	.0344	.0250	2750	2056
22	30,000	0.808	624	959	467	43.40	2839	4340	0.0468	0.0390	4366	3280
23		.808	625	958	465	43.58	2748	4010	.0438	.0363	4251	3185
24		.809	623	958	465	43.58	2638	3650	.0408	.0317	4114	3025
25		.808	628	961	465	43.68	2473	3280	.0371	.0277	3845	2757
26		.806	625	959	464	43.67	2277	3045	.0344	.0252	3543	2456
27	35,000	0.625	495	640	427	30.31	2045	3115	0.0480	0.0404	2919	2347
28		.619	495	640	422	30.54	1998	2940	.0457	.0375	2882	2312
29		.613	496	639	419	30.53	1955	2625	.0422	.0331	2748	2185
30		.607	497	638	421	30.50	1856	2440	.0398	.0303	2625	2067
31	40,000	0.613	389	501	422	23.86	1619	2460	0.0487	0.0412	2303	1865
32		.608	385	504	425	23.46	1580	2310	.0468	.0387	2250	1817
33		.603	390	499	423	23.70	1519	2120	.0433	.0344	2180	1727
34		.616	388	503	423	23.80	1420	1849	.0381	.0295	2009	1569
35	45,000	0.613	305	394	425	18.22	1260	2017	0.0515	0.0445	1785	1444
36		.611	307	395	426	18.17	1238	1902	.0493	.0418	1754	1417
37		.600	309	394	424	18.32	1220	1748	.0460	.0378	1708	1373
38		.616	307	397	423	18.33	1200	1695	.0450	.0365	1676	1335

TABLE I - Concluded. AFTERBURNER PERFORMANCE DATA

Run	Specific fuel consumption W_f/F_n (lb/(hr)(lb thrust))	Turbine-outlet total pressure P_5 (lb/sq ft abs)	Turbine-outlet total temperature T_5 (°R)	Manufacturer's turbine-outlet indicated temperature $T_{5,i}$ (°R)	Combustion-chamber-inlet static pressure P_6 (lb/sq ft abs)	Combustion-chamber-inlet velocity V_6 (ft/sec)	Exhaust-nozzle-inlet total pressure P_9 (lb/sq ft abs)	Exhaust-gas total temperature T_n (°R)	Afterburner combustion efficiency η_b	Engine combustion efficiency η_e
				Configuration A						
1	2.477	1810	1780	1763	1665	485	1646	3347	0.789	0.978
2	2.241	1757	1730	1698	1608	469	1601	3064	.828	.985
3	2.214	1755	1720	1680	1601	462	1598	3103	.888	.985
4	2.148	1694	1668	1634	1538	461	1540	2897	.885	.985
5	2.405	1144	1753	1777	1054	468	1040	3309	0.900	0.920
6	2.257	1146	1723	1720	1054	458	1042	3270	.870	.937
7	2.246	1129	1710	1701	1033	465	1023	3106	.836	.958
8	2.198	1114	1699	1678	1020	463	1013	3099	.868	.958
9	2.186	1093	1686	1646	998	456	992	3013	.876	.962
				Configuration C						
10	2.298	3333	1700	1702	3015	498	3086	2761	0.855	0.985
11	2.254	3263	1673	1666	2933	507	3028	2647	.856	.985
12	2.447	3027	1544	1555	2891	507	2789	2238	.670	.985
13	2.515	2883	1475	1496	2540	513	2664	2032	.593	.985
14	2.205	1565	1765	1787	1438	486	1454	3238	0.902	0.976
15	2.102	1517	1706	1728	1391	485	1410	3020	.919	.984
16	2.058	1476	1672	1689	1350	486	1372	2884	.918	.985
17	2.055	1427	1610	1629	1301	485	1328	2867	.870	.982
18	2.206	1759	1780	1778	1615	491	1634	3198	0.898	0.985
19	2.158	1678	1723	1735	1536	492	1557	3027	.906	.985
20	2.106	1636	1667	1676	1492	492	1517	2826	.889	.985
21	2.230	1487	1530	1557	1340	497	1377	2338	.700	.985
22	2.189	2007	1780	1789	1832	498	1850	3212	0.919	0.985
23	2.135	1975	1735	1750	1800	496	1818	3083	.928	.985
24	2.079	1930	1698	1700	1760	494	1777	2951	.937	.985
25	2.079	1848	1625	1635	1673	497	1704	2685	.871	.985
26	2.167	1750	1542	1547	1573	524	1616	2395	.741	.985
27	2.199	1407	1745	1790	1296	488	1308	3208	0.899	0.974
28	2.136	1397	1712	1751	1285	488	1297	3117	.911	.975
29	2.101	1358	1670	1699	1244	487	1259	2940	.904	.974
30	2.078	1318	1640	1653	1207	491	1224	2782	.869	.984
31	2.187	1109	1720	1774	1028	475	1030	3271	0.923	0.943
32	2.141	1098	1702	1748	1014	472	1018	3252	.964	.941
33	2.115	1066	1673	1717	987	460	990	3015	.918	.983
34	2.083	1018	1587	1647	938	476	945	2759	.879	.947
35	2.269	867	1715	1781	811	485	802	3311	0.880	0.908
36	2.216	857	1700	1760	814	459	795	3276	.909	.907
37	2.160	848	1668	1723	800	---	784	3127	.910	.908
38	2.167	838	1660	1711	789	463	774	3048	.888	.913

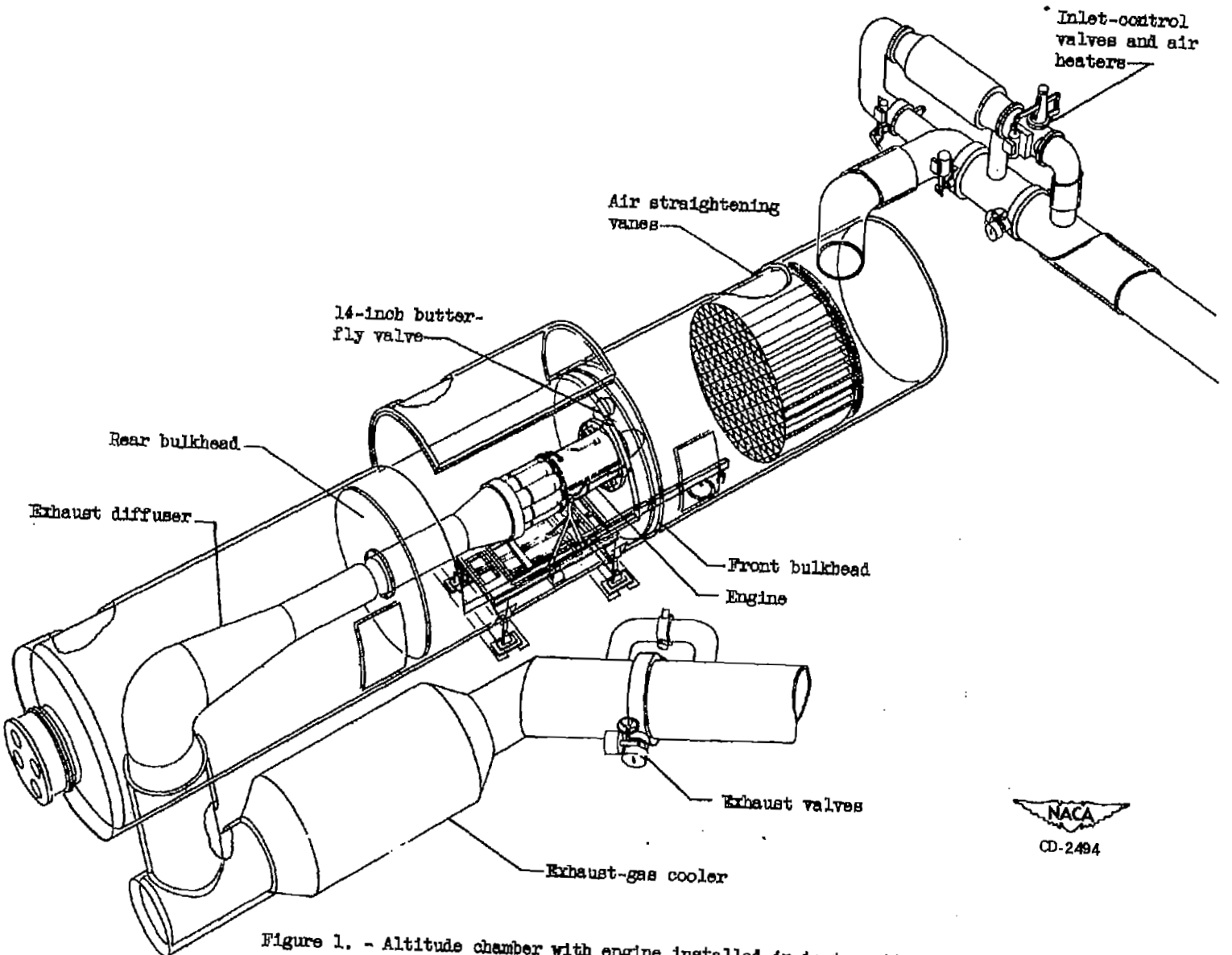

Figure 1. - Altitude chamber with engine installed in test section.

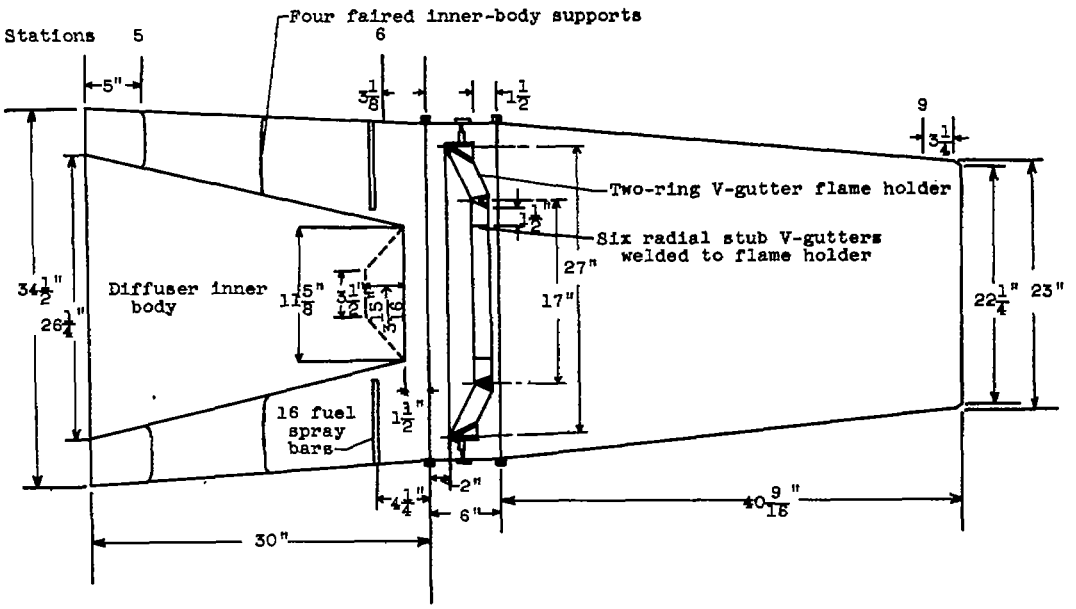

(a) Configuration A.

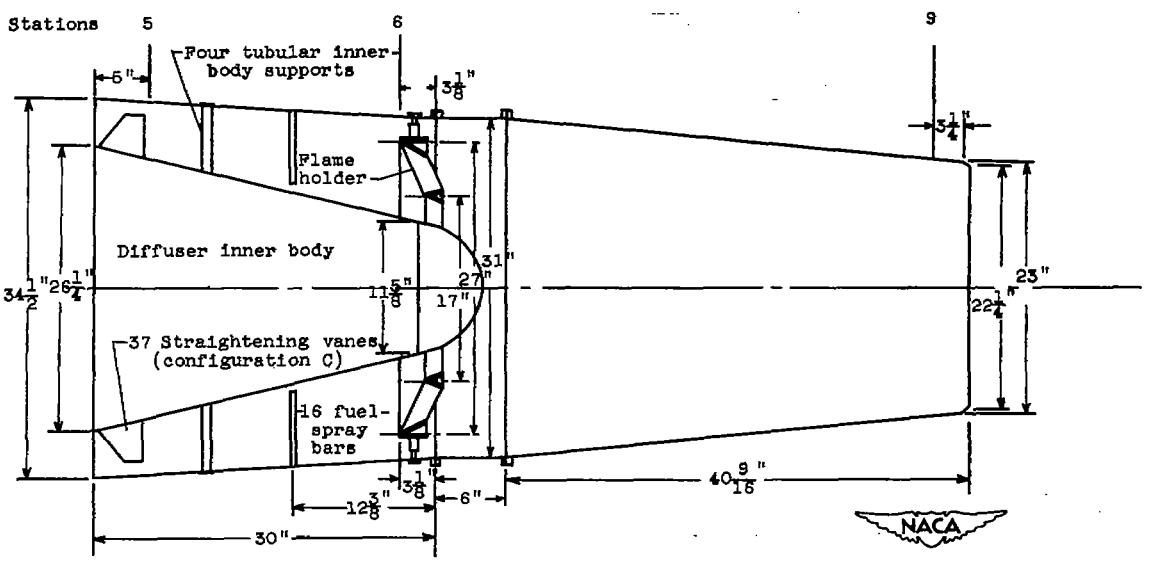

(b) Configurations B and C.

Figure 2. - Cross section of afterburner installation.

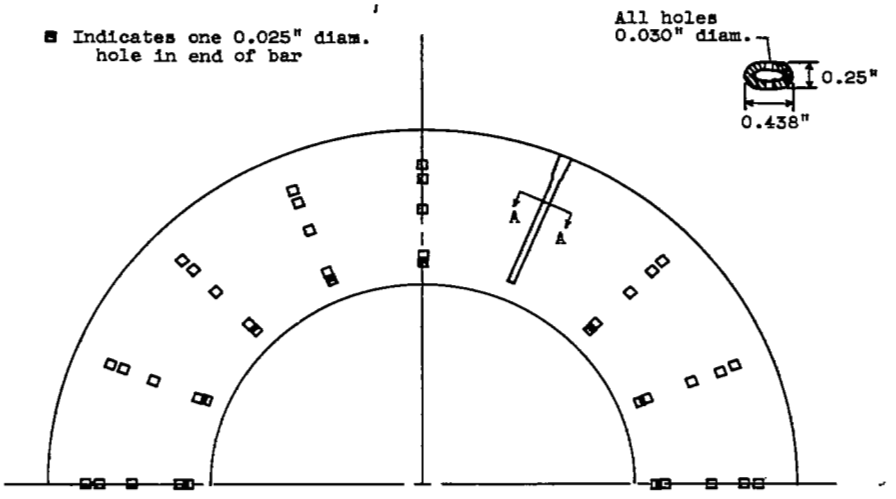

(a) Fuel system used in configuration A, located 6¼ inches upstream of flame holder.

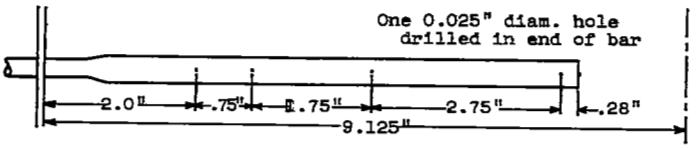

(b) Fuel-spray bar used in configuration A.

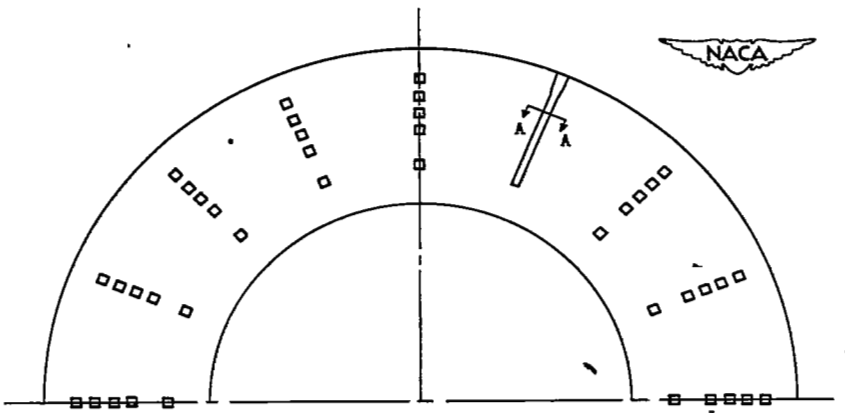

(c) Fuel system used in configurations B and C, located 9¼ inches upstream of flame holder.

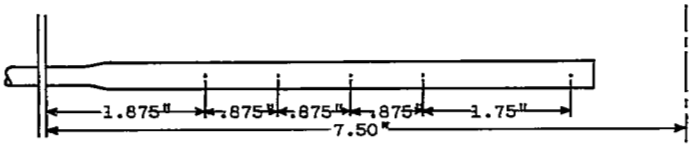

(d) Fuel-spray bar used in configurations B and C.

Figure 3. - Schematic diagrams of fuel systems.

[redacted]

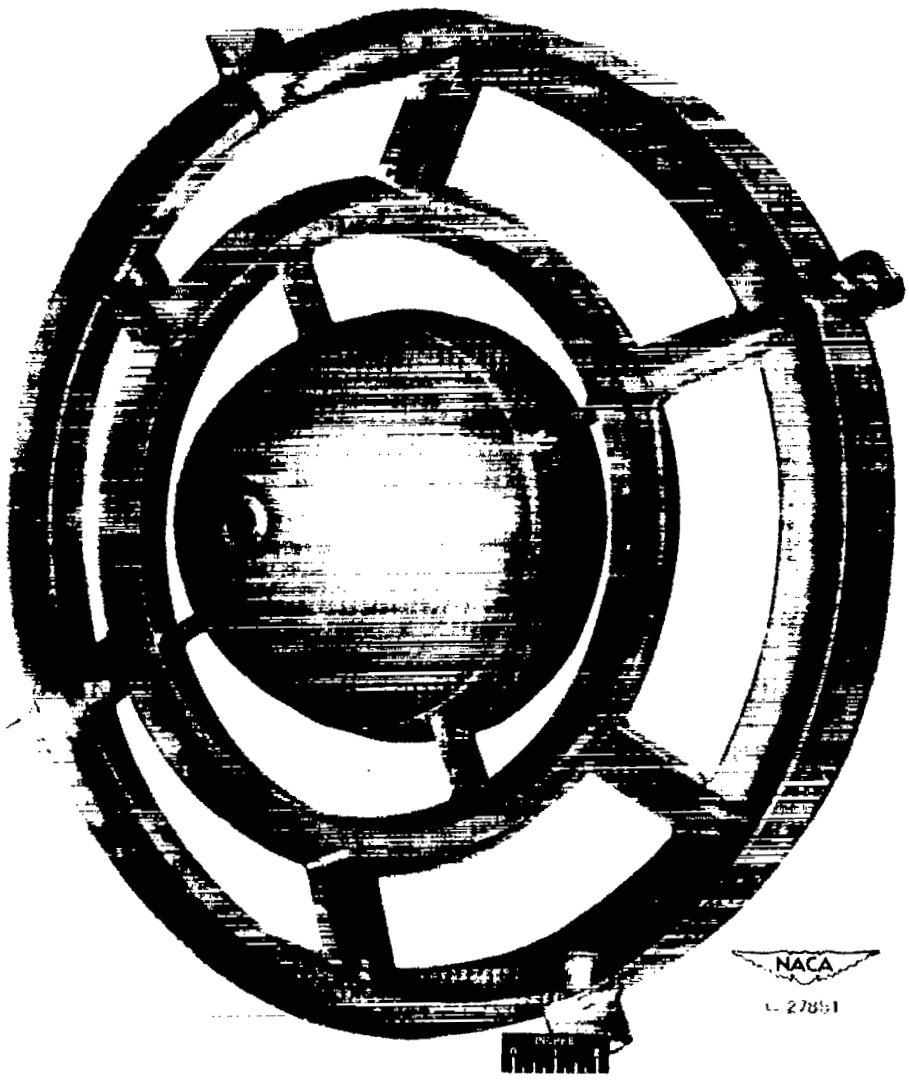

Figure 4. - Flame holder used for configurations B and C.

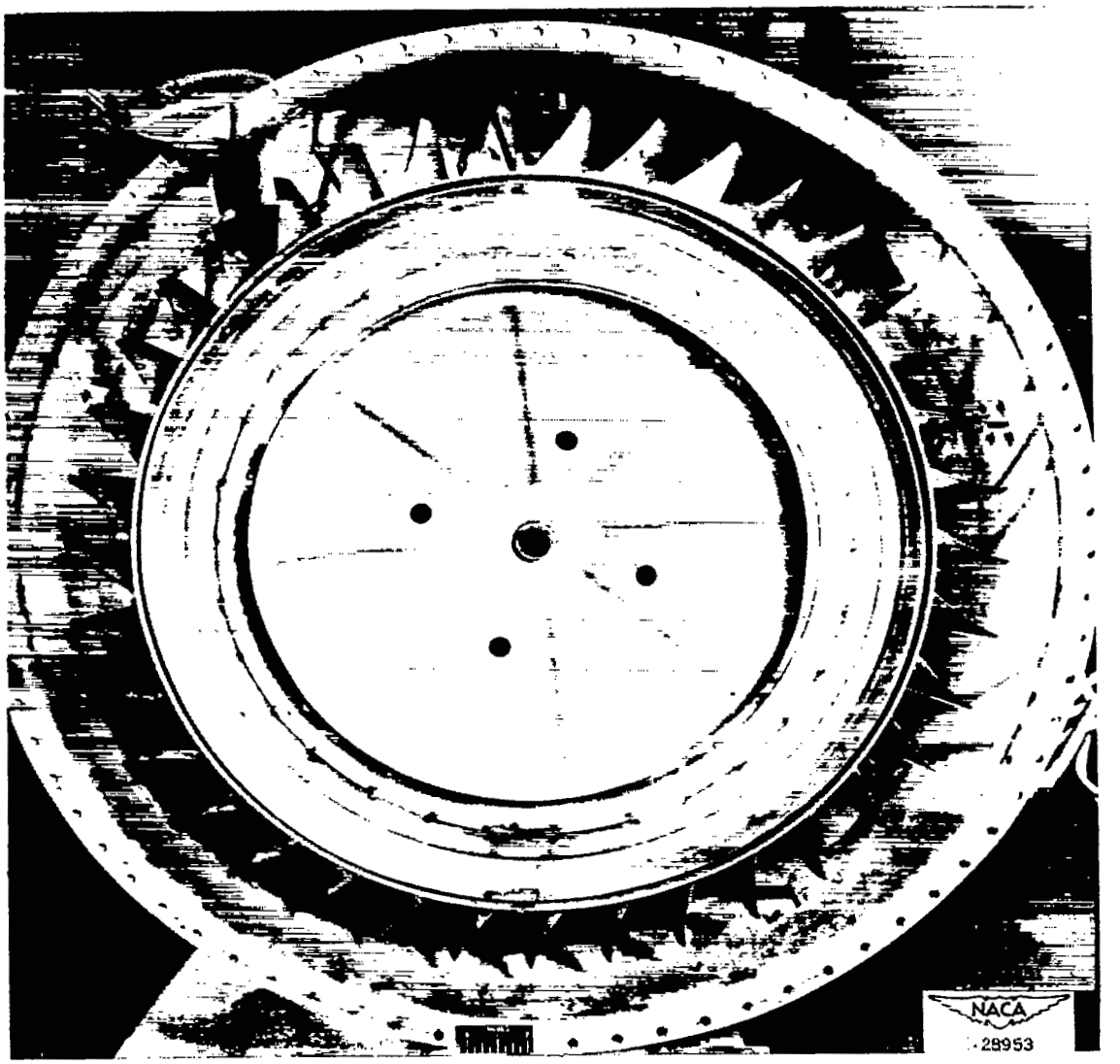

(a) Installed straightening vanes.

Figure 5. - Turbine-outlet straightening vanes used in configuration C.

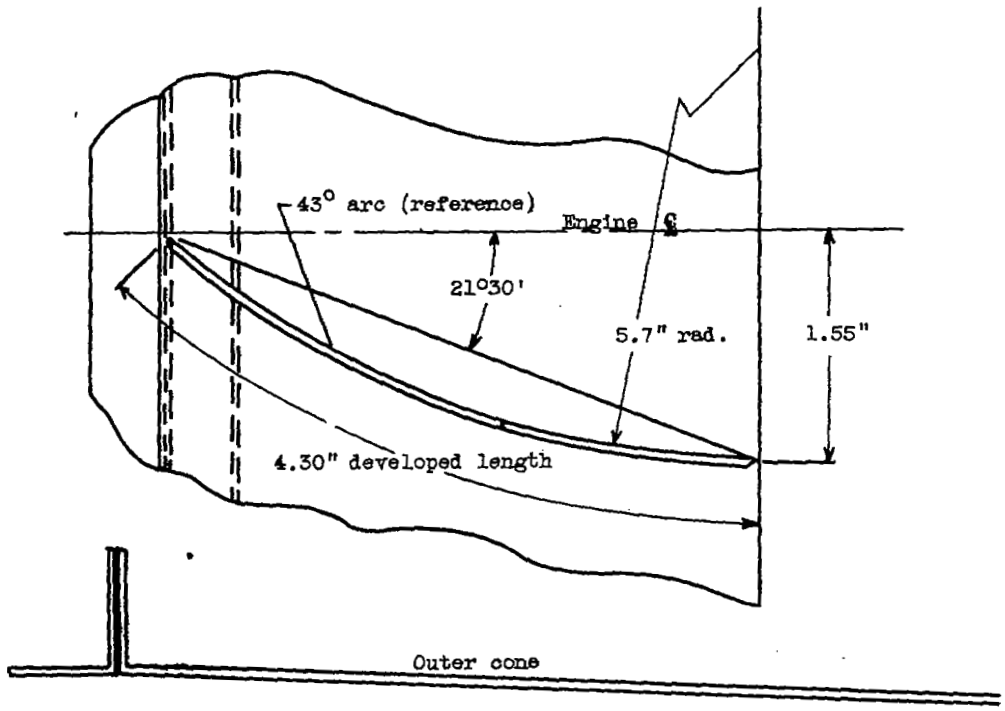

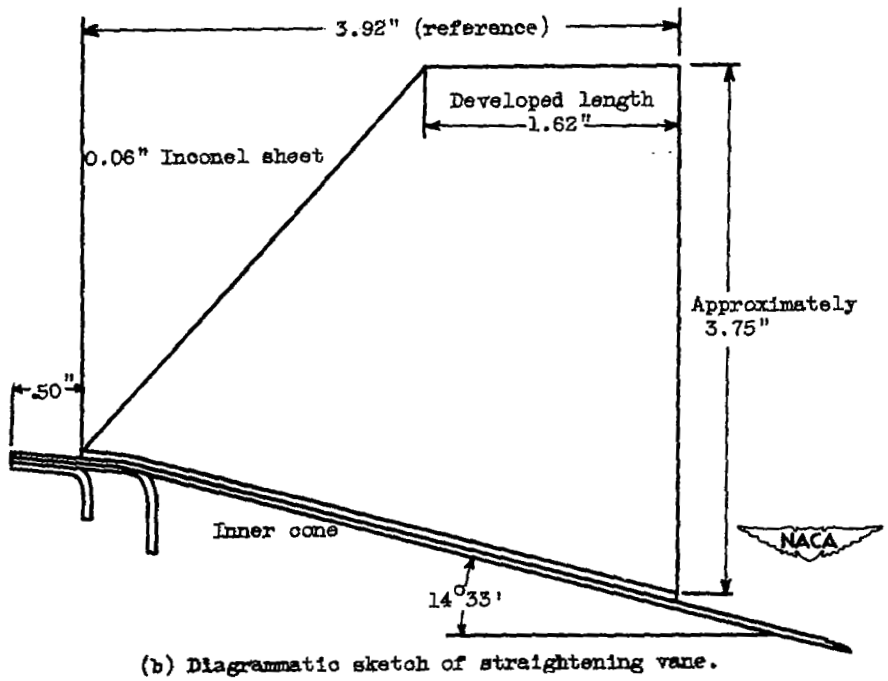

(b) Diagrammatic sketch of straightening vane.

Figure 5. - Concluded. Turbine-outlet straightening vanes used in configuration C.

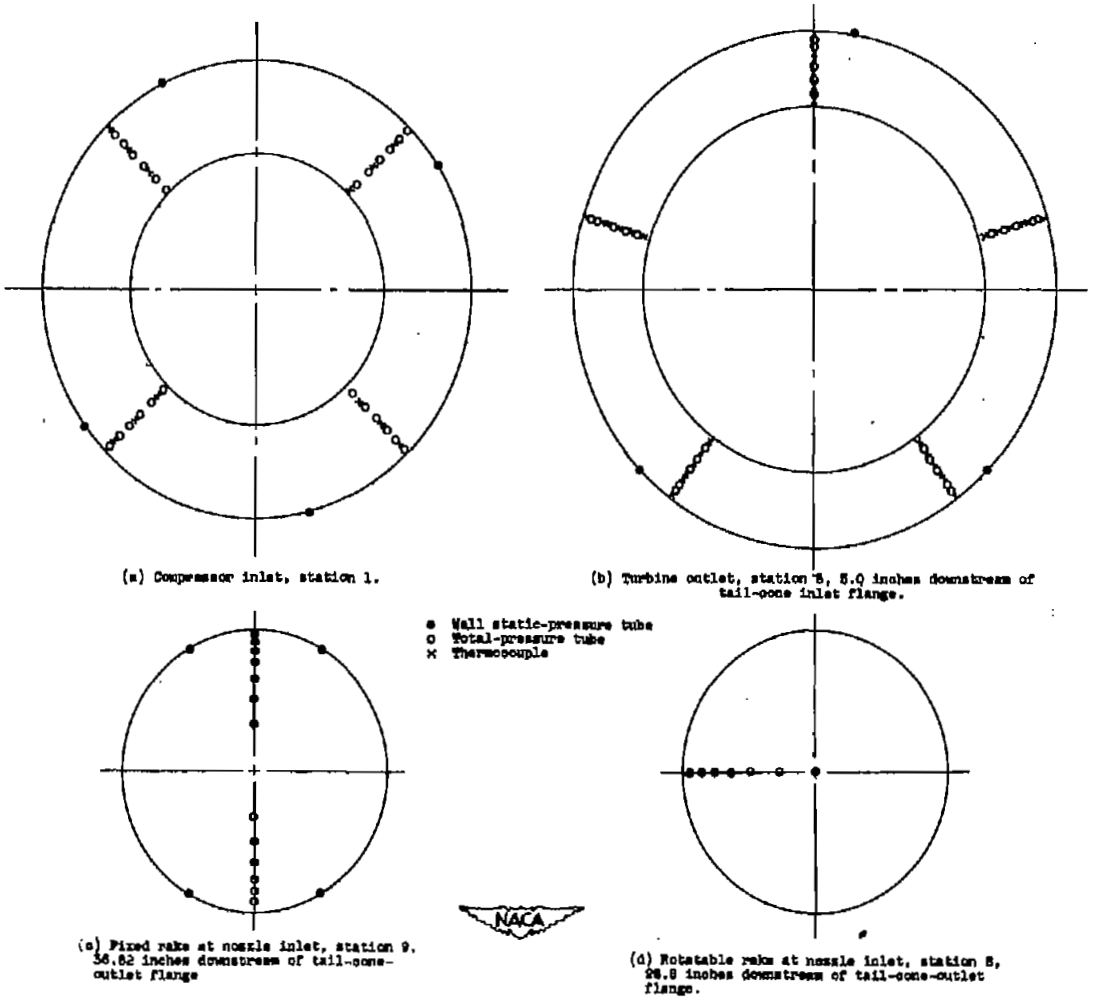

Figure 6. - Cross section of instrumentation as installed in engine and afterburner.

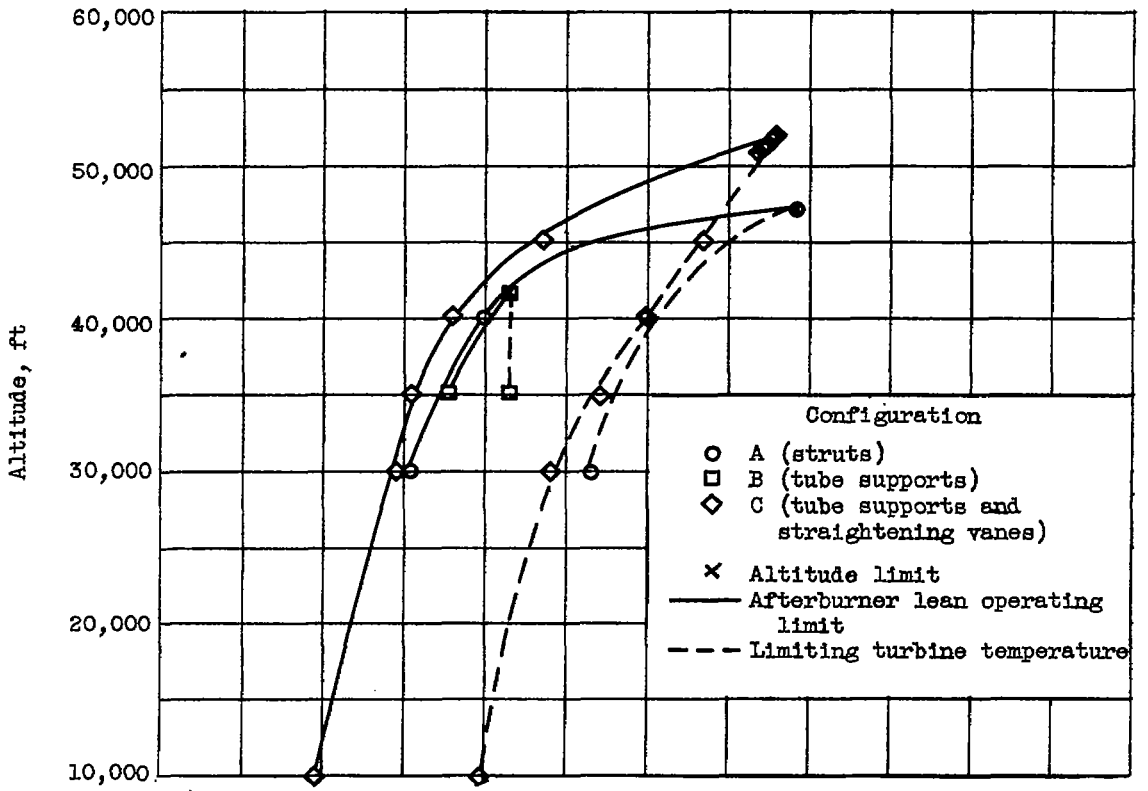

(a) Variation of operational limits with altitude; flight Mach number, 0.6.

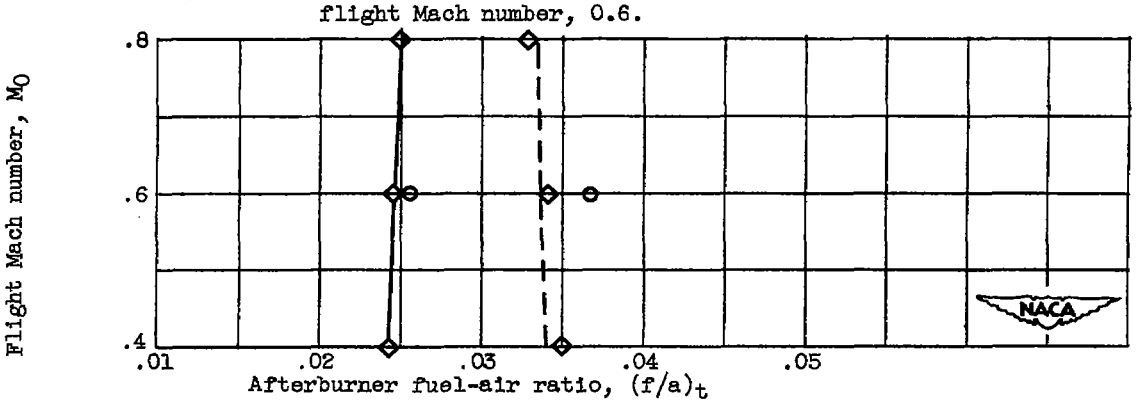

(b) Variation of operational limits with flight Mach number; altitude, 30,000 feet.

Figure 7. - Operating limits of afterburner configurations. Engine speed, 8000 rpm.

[redacted]

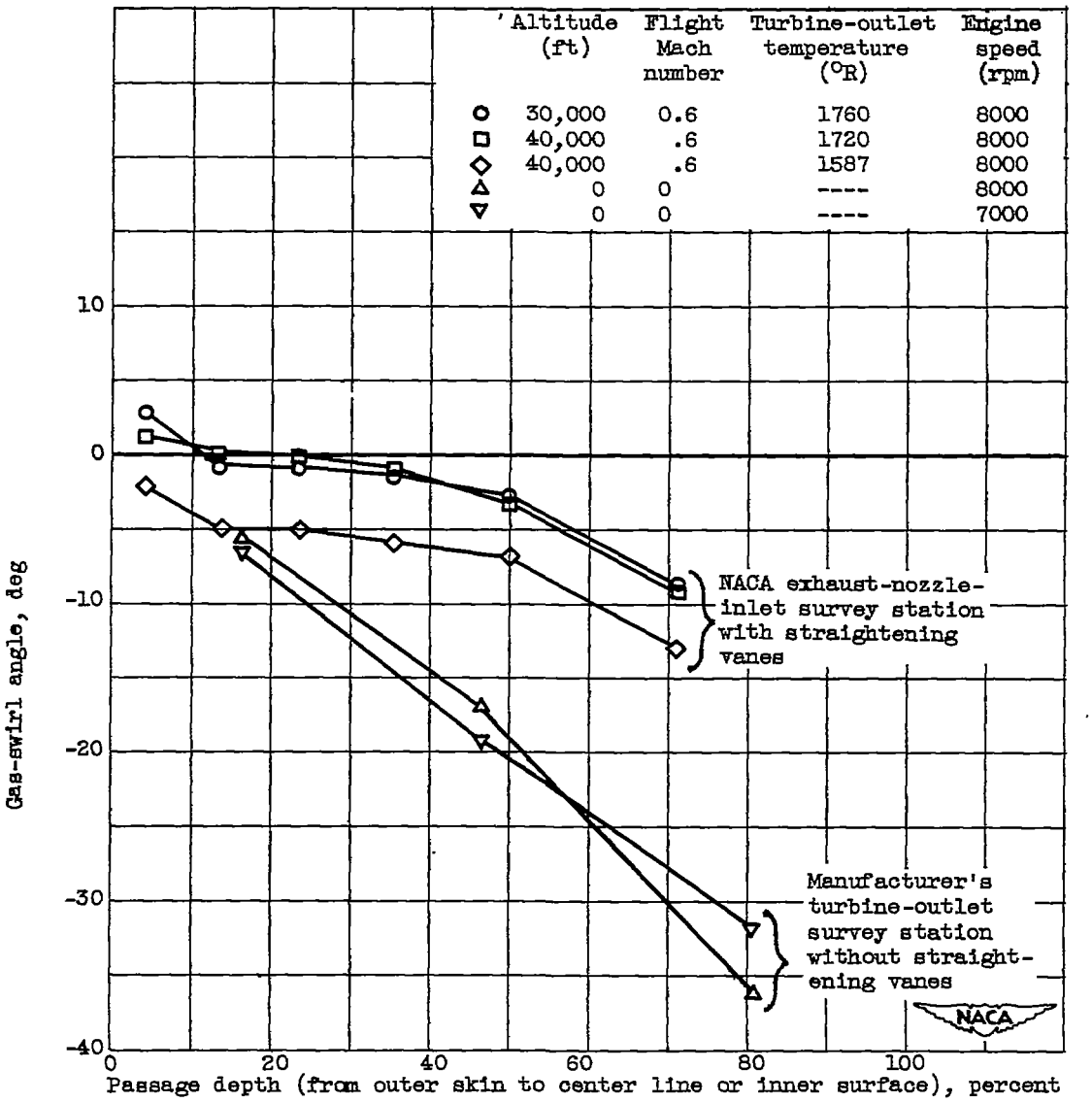

(a) Variation of swirl angle of tail-pipe gas flow with passage depth for various flight conditions. (Gas-swirl angle is positive when gas rotation is in same direction as engine rotation.)

Figure 8. - Gas-flow-swirl conditions in afterburner for configuration C.

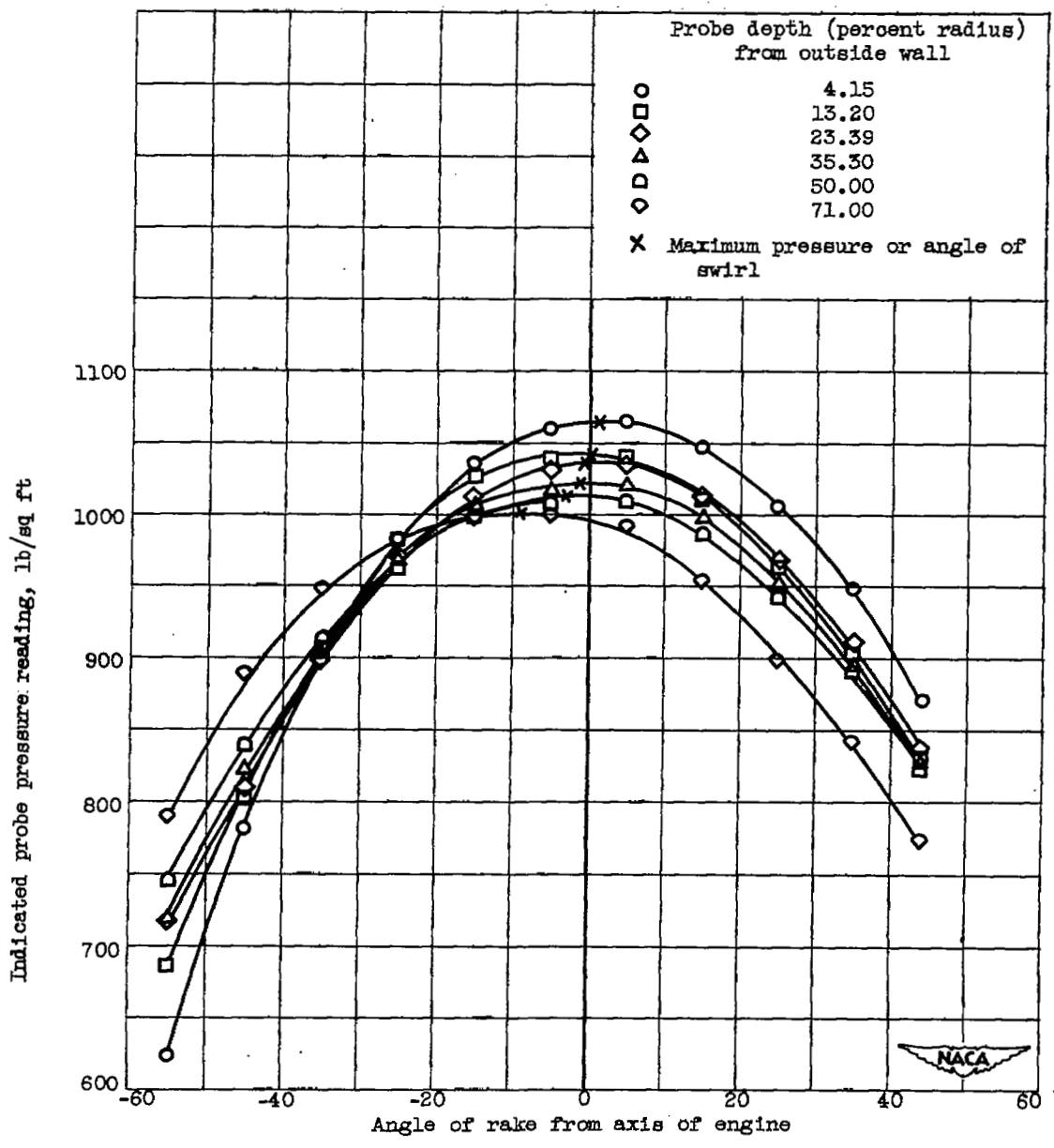

(b) Typical rotating rake data. Altitude, 40,000 feet; flight Mach number, 0.6; turbine-outlet temperature, 1720° R. (Gas-swirl angle is positive when gas rotation is in same direction as engine rotation.)

Figure 8. - Concluded. Gas-flow swirl conditions in afterburner for configuration C.

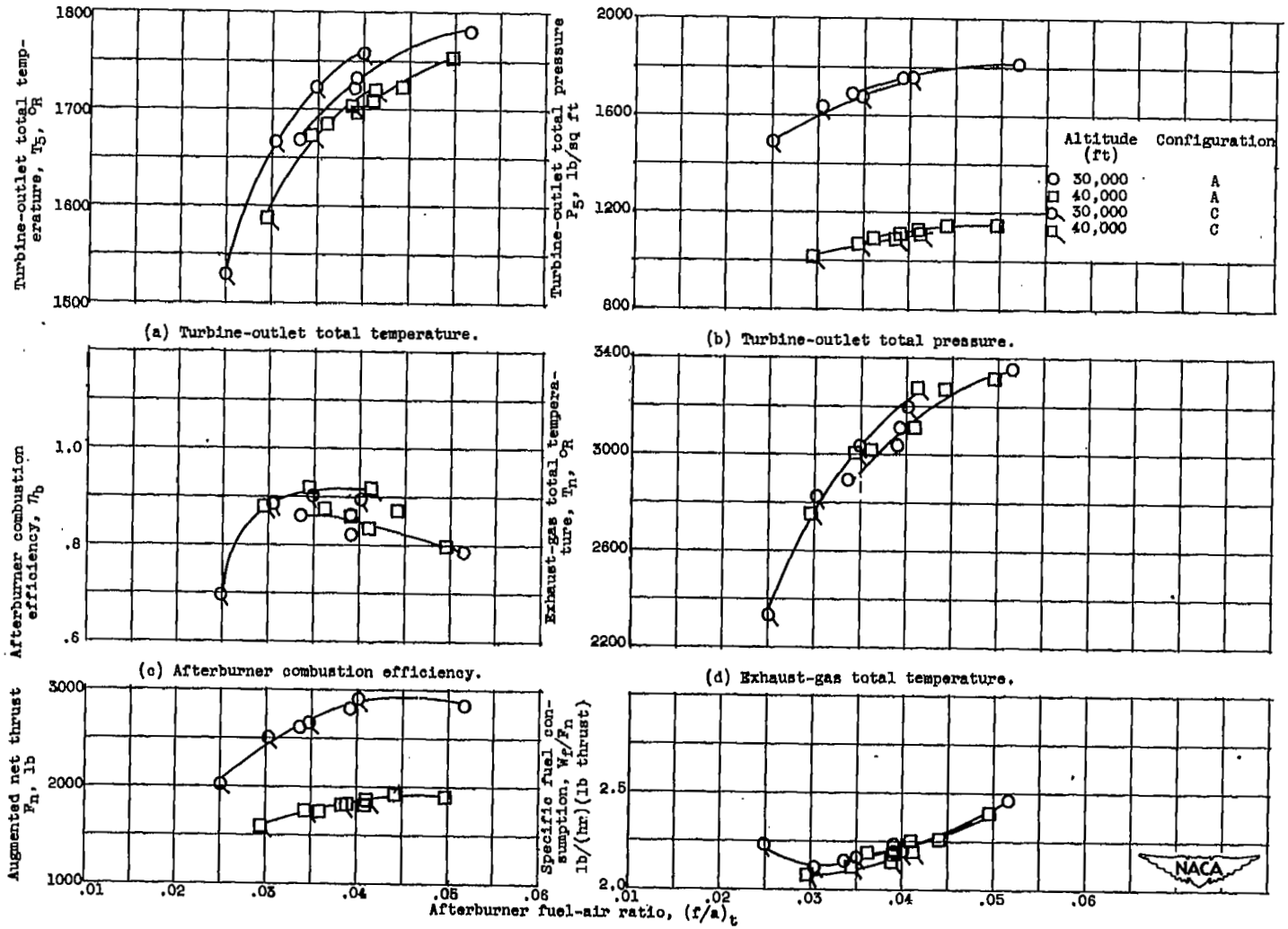

(a) Turbine-outlet total temperature.

(b) Turbine-outlet total pressure.

(c) Afterburner combustion efficiency.

(d) Exhaust-gas total temperature.

(e) Augmented net thrust.

(f) Specific fuel consumption.

Figure 9. - Effect of internal afterburner configuration changes on variation of performance with afterburner fuel-air ratio for flight Mach number of 0.6. Engine speed, 8000 rpm.

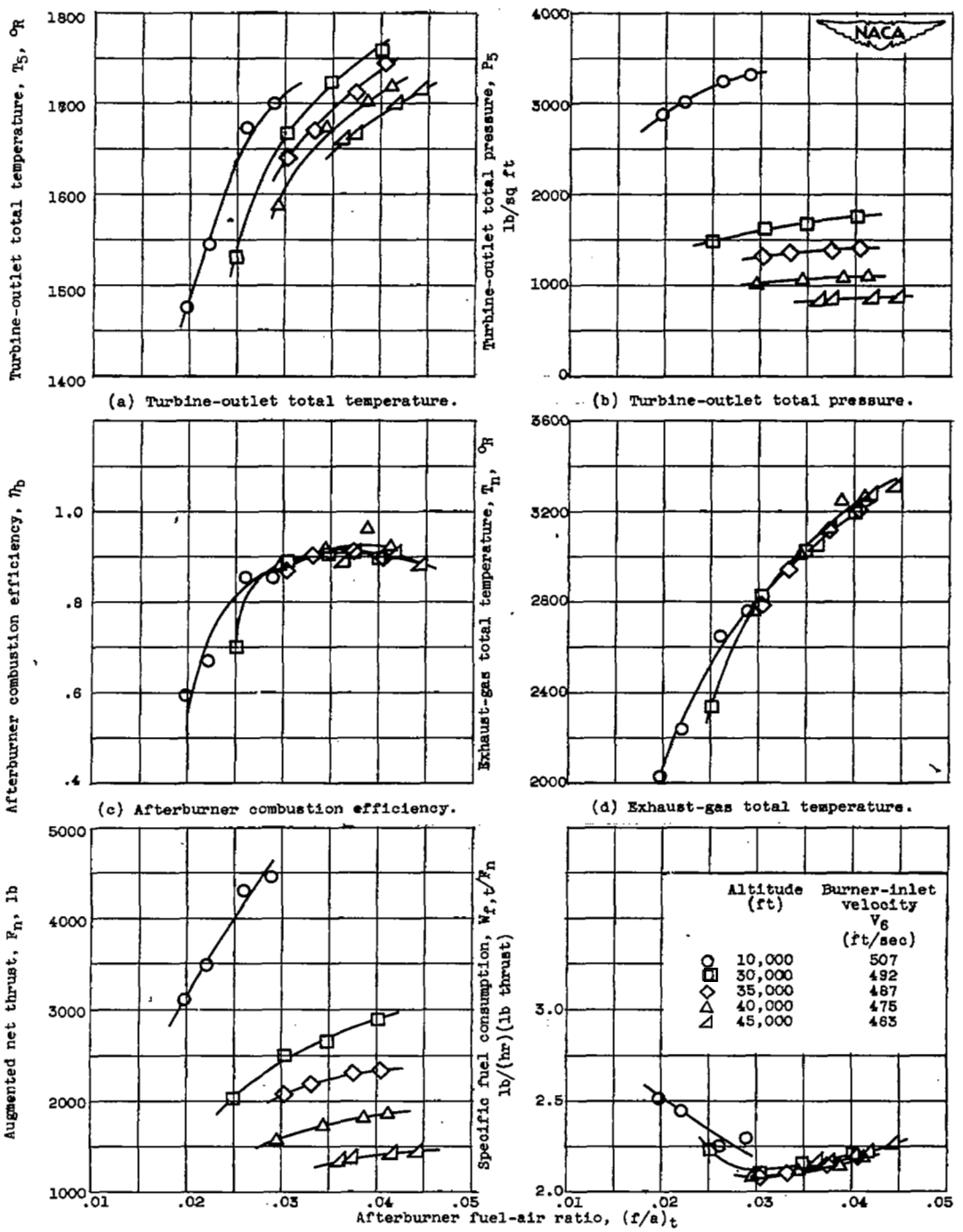

Figure 10. - Effect of altitude on variation of performance of configuration C with afterburner fuel-air ratio. Flight Mach number, 0.6; engine speed, 8000 rpm.

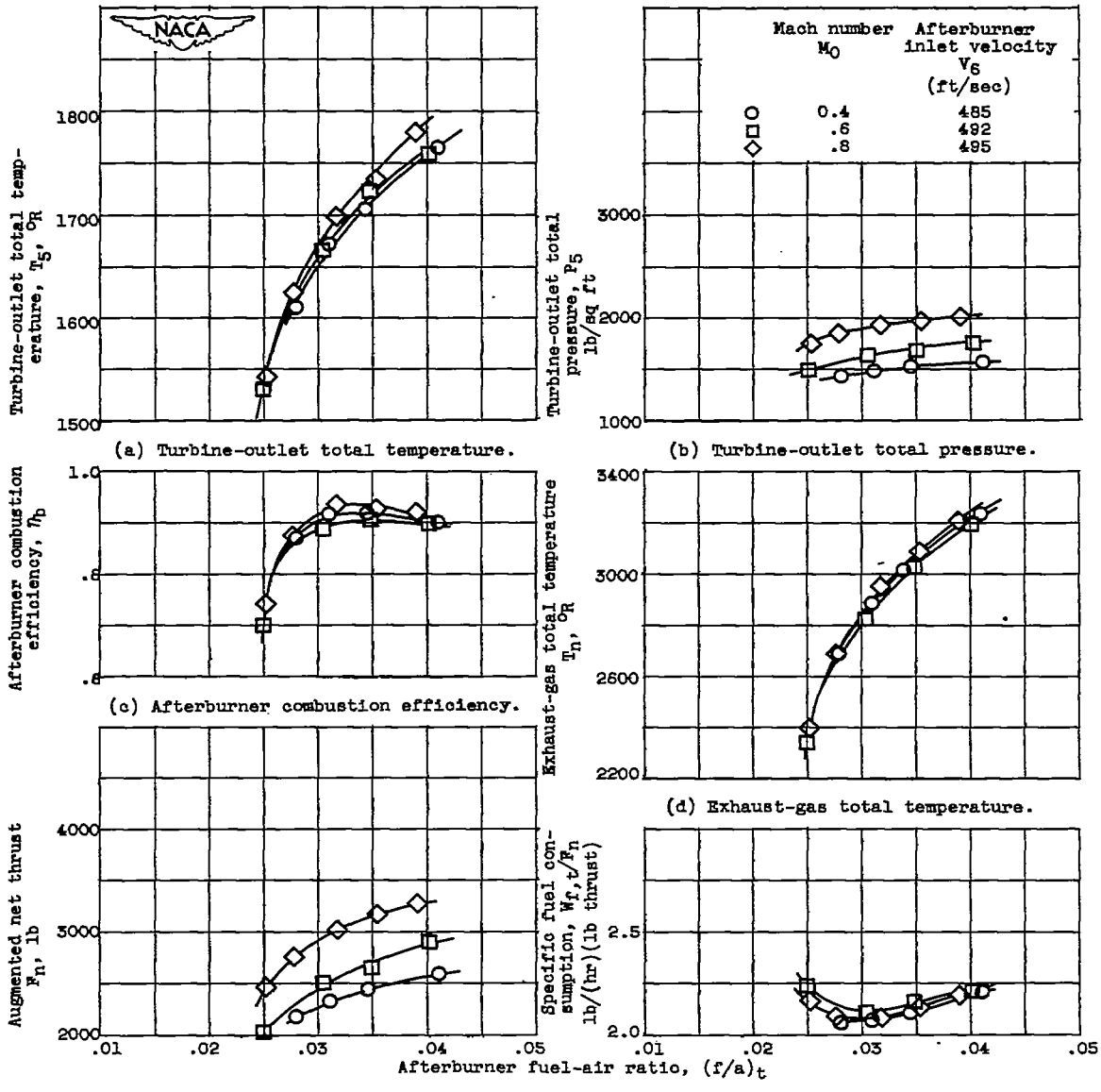

(a) Turbine-outlet total temperature.

(b) Turbine-outlet total pressure.

(c) Afterburner combustion efficiency.

(d) Exhaust-gas total temperature.

(e) Augmented net thrust.

(f) Specific fuel consumption.

Figure 11. - Effect of Mach number on variation of performance of configuration C with afterburner fuel-air ratio. Altitude, 30,000 feet; engine speed, 8000 rpm.

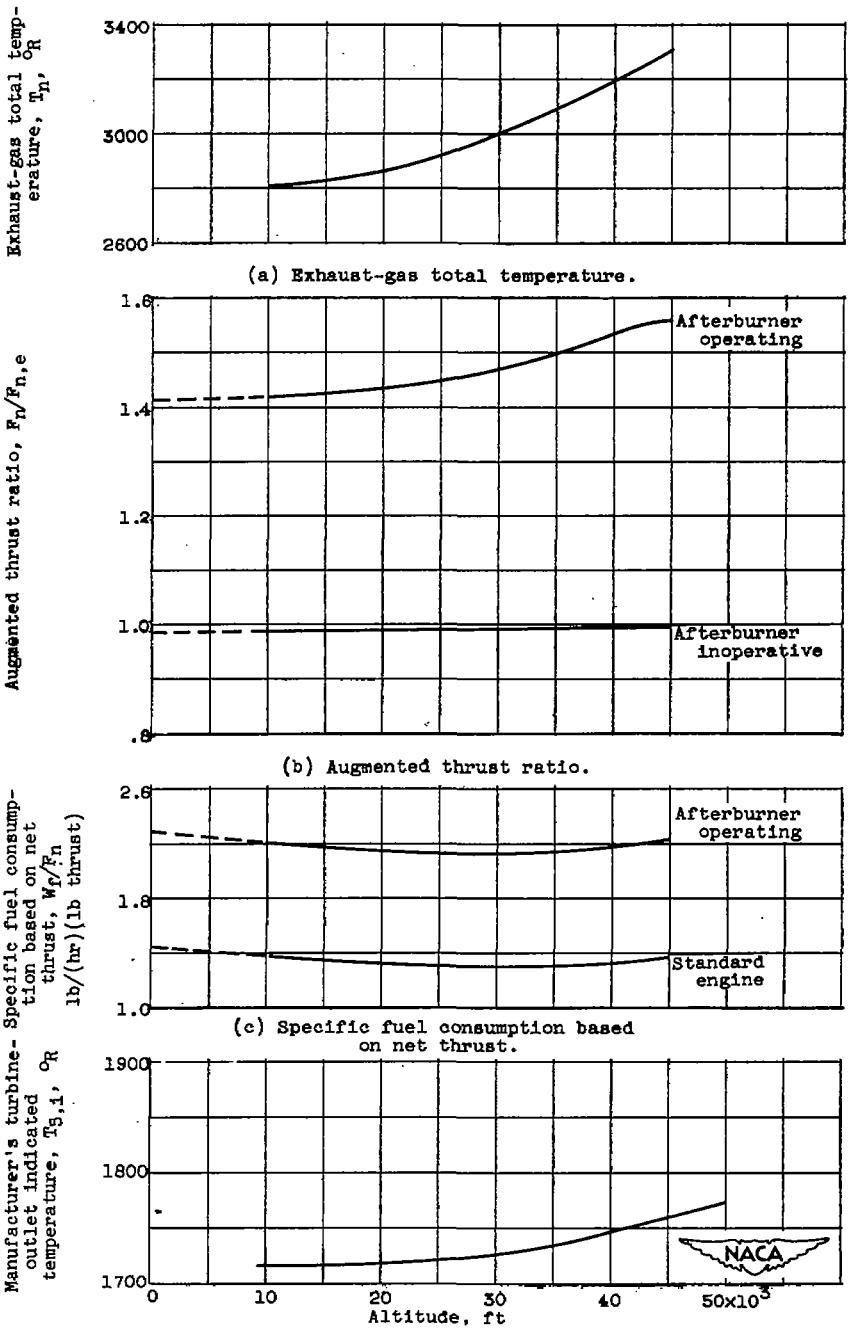

(a) Exhaust-gas total temperature.

(b) Augmented thrust ratio.

(c) Specific fuel consumption based on net thrust.

(d) Variation of manufacturer's indicated turbine-outlet temperature with altitude, NACA turbine-outlet gas temperature of 1710° R.

Figure 12. - Variation of afterburner performance characteristics of configuration C with altitude. Turbine-outlet total temperature, 1710° R; Mach number, 0.6; engine speed, 8000 rpm.

5S

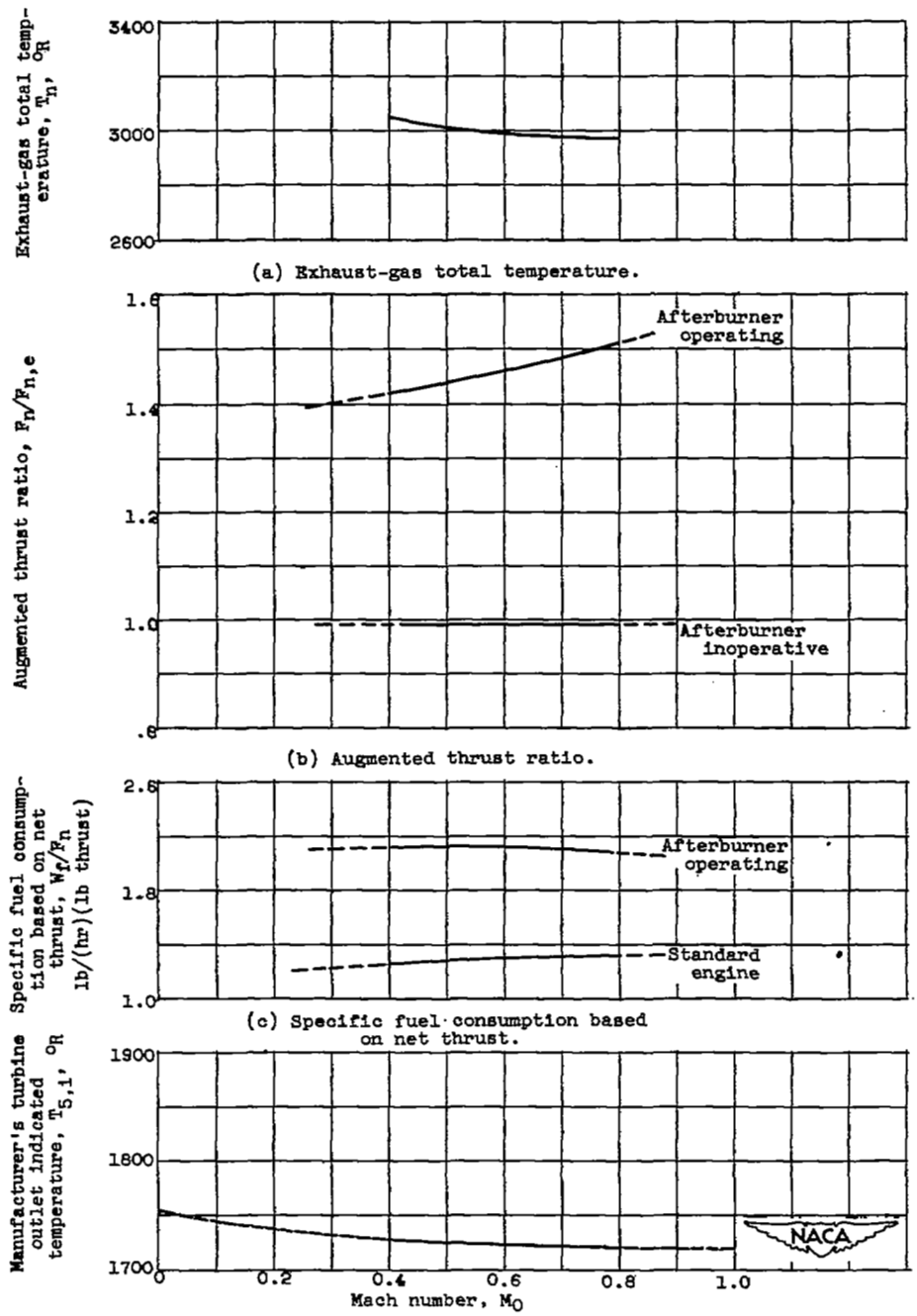

(a) Exhaust-gas total temperature.

(b) Augmented thrust ratio.

(c) Specific fuel consumption based on net thrust.

(d) Variation of manufacturer's indicated turbine-outlet temperature with Mach number for NACA turbine-outlet gas temperature of 1710° R.

Figure 13. - Variation of afterburner performance characteristics of configuration C with Mach number. Turbine-outlet total temperature, 1710° R; altitude 30,000 feet; engine speed, 8000 rpm.